CHAPTER FOUR

Electronic Structures of Molecules and Solids

4.1 Introduction

Solid state materials are often classified according to how their electrical resistivity r varies as a function of temperature T. Metals and semiconductors have positive and negative slopes in their ρ-versus-T plots, respectively (*Figures 4.1a* and *4.1b*). For some compounds, metallic states are stable

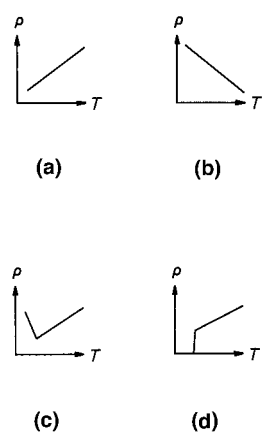

Figure 4.1. Schematic resistivity-versus-temperature plots for (a) a metal, (b) a semiconductor, (c) a metal undergoing a metal-to-semiconductor phase transition, and (d) a metal undergoing a metal-to-superconductor phase transition.

only in a certain region of temperature so that a metal may become a semiconductor (*Figure 4.1c*) or a superconductor (*Figure 4.1d*) when the temperature is lowered. In understanding such a phase transition of solid-state materials, it is crucial to know their electronic structures.

The electronic structure of a molecule is characterized by discrete energy levels (*Figure 4.2a*), and that of a solid by energy bands (*Figure 4.2b*). As illustrated in *Figure 4.2c*, any given energy band consists of N discrete levels, where N is the total number of unit cells in a solid. For all practical purposes, all energy levels falling within a band are allowed because $N \rightarrow \infty$. In a one-electron picture of electronic structure, each band level is filled with two electrons. At T = 0 K a normal semiconductor contains only completely filled and completely empty bands (*Figure 4.2d*), so an energy gap (i.e., band gap E_g) exists between the highest occupied and the lowest unoccupied band levels. A normal insulator has a band gap larger than 2 eV. A normal metal has at least one partially filled band (*Figure 4.2e*), so there is no energy gap between the highest occupied level (i.e., the Fermi level e_f) and the lowest unoccupied level.

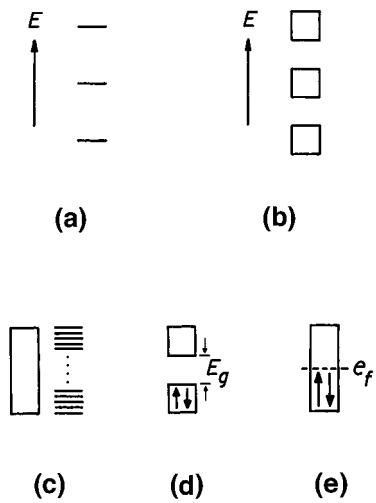

Figure 4.2. (a) Discrete energy levels of a molecule. (b) Energy bands of a solid. (c) Schematic view of an energy band in terms of closely-spaced discrete energy levels. (d) Band occupancy expected for a normal semiconductor. (e) Band occupancy expected for a normal metal.

The above discussion is based on one-electron theory, which neglects electron localization resulting from electron-electron repulsion, electron-phonon interaction or random potentials.[1] Magnetic insulators possess unpaired energy levels. Within a one-electron picture, these systems also possess partially filled bands. However, the way the band levels are filled in magnetic insulators is different from that in normal metals (see *Section 4.6.1* for further discussion).[2] *Therefore, when a solid system is predicted to be metallic by one-electron electronic band structure calculations, it is extremely important to recall that such a system may not be a metal but a magnetic insulator. The metallic versus magnetic insulating state of a solid is similar in nature to the low-spin versus high-spin state of a molecule.*[2]

4.2 Electronic structures of molecules

4.2.1 Molecular orbital theory

In molecular orbital (MO) theory, the electronic structure of a molecule is described by molecular orbitals ψ_i (i = 1, 2, ···, m) that are expressed as a linear combination of atomic orbitals χ_μ (μ = 1, 2, ···, m),

$$\psi_i = \sum_\mu C_{\mu i}\ \chi_\mu \tag{4.1}$$

where $C_{\mu i}$ is the coefficient of the atomic orbital χ_μ. The energies e_i of the MO's ψ_i are eigenvalues associated with the effective Hamiltonian H^{eff}

$$H^{eff}\ \psi_i = e_i\ \psi_i \tag{4.2}$$

so that e_i is written as

$$e_i = \frac{\langle \psi_i | H^{eff} | \psi_i \rangle}{\langle \psi_i | \psi_i \rangle} \tag{4.3}$$

The energy e_i is optimum with respect to changes in the coefficients $C_{\kappa i}$ so that

$$\frac{\partial e_i}{\partial C_{\kappa i}} = 0 \qquad (\kappa = 1, 2, \cdots, m) \tag{4.4}$$

which leads to the m x m secular determinant

$$\begin{vmatrix} H_{11} - e_i S_{11} & H_{12} - e_i S_{12} & \bullet & \bullet & H_{1m} - e_i S_{1m} \\ H_{21} - e_i S_{21} & H_{22} - e_i S_{22} & \bullet & \bullet & H_{2m} - e_i S_{2m} \\ \bullet & \bullet & \bullet & \bullet & \bullet \\ \bullet & \bullet & \bullet & \bullet & \bullet \\ H_{m1} - e_i S_{m1} & H_{m2} - e_i S_{m2} & \bullet & \bullet & H_{mm} - e_i S_{mm} \end{vmatrix} = 0 \tag{4.5}$$

where the matrix elements $H_{\mu\nu}$ and $S_{\mu\nu}$ are expressed as

$$H_{\mu\nu} = \langle \chi_\mu | H^{eff} | \chi_\nu \rangle \tag{4.6}$$

$$S_{\mu\nu} = \langle \chi_\mu | \chi_\nu \rangle \tag{4.7}$$

The matrix elements $H_{\mu\nu}$, $S_{\mu\nu}$ and $C_{\mu i}$ (μ, ν, i = 1, 2, ···, m) form m x m matrices **H**, **S** and **C**, respectively. These matrices are related by the pseudo-eigenvalue equation,

$$\mathbf{HC} = \mathbf{SCe} \tag{4.8}$$

where **e** is an m x m diagonal matrix with its diagonal elements given by e_i (i = 1, ···, m). Thus if the matrices **H** and **S** are determined, then the coefficient matrix **C** and orbital energies **e** are obtained by solving the pseudo-eigenvalue problem, Eq. 4.8. If the overlap matrix **S** is approximated by the unit matrix **1**, then Eq. 4.8 is simplified as

$$\mathbf{HC} = \mathbf{Ce} \tag{4.9}$$

4.2.2 Population analysis

Each MO ψ_i can be occupied by n_i electrons (n_i = 2, 1 or 0) so that the total number of electrons N_{elec} of a molecule is written as

$$N_{elec} = \sum_i n_i \langle \psi_i | \psi_i \rangle \tag{4.10}$$

because each MO is normalized to unity, i.e., $\langle \psi_i | \psi_i \rangle = 1$. This leads to the Mulliken population analysis, which partitions the N_{elec} electrons of a molecule into its atoms and bonds. The net population $p_{\mu\mu}$ of an atomic orbital χ_μ is defined by

$$p_{\mu\mu} = \sum_i n_i \left(C_{\mu i}\right)^2, \tag{4.11}$$

the overlap population $p_{\mu\nu}$ between atomic orbitals χ_μ and χ_ν by

$$p_{\mu\nu} = \sum_i 2\, n_i C_{\mu i} C_{\nu i} S_{\mu\nu}, \tag{4.12}$$

and the gross population q_μ of an atomic orbital χ_μ by

$$q_\mu = p_{\mu\mu} + 0.5 \sum_{\nu(\neq\mu)} p_{\mu\nu} \tag{4.13}$$

Thus the gross population Q_A of atom A (i.e., the number of electrons on A) is given by

$$Q_A = \sum_{\mu \in A} q_\mu \tag{4.14}$$

so that the net charge on atom A is $Z_A - Q_A$, where Z_A is the effective nuclear charge of A (i.e., the nuclear charge minus the number of the core electrons). The overlap population P_{AB} between atoms A and B (i.e., the number of electrons in the bond A-B) is given by

$$P_{AB} = \sum_{\mu \in A} \sum_{\nu \in B} p_{\mu\nu} \tag{4.15}$$

4.2.3 Fragment molecular orbital analysis [3]

It is often convenient to consider a molecule in terms of its fragments (e.g., ethane CH_3CH_3 in terms of two methyl groups CH_3). In MO theory this amounts to expressing the MO's of a molecule AB in terms of the MO's of its fragments A and B, i.e., in terms of the fragment molecular orbitals (FMO's). For convenience of discussion, consider that the set of atomic orbitals $\{\chi_1, \chi_2, \cdots, \chi_n, \chi_{n+1}, \chi_{n+2}, \cdots, c_m)$ describing the molecule AB are arranged such that

$$\begin{aligned} &\chi_1, \chi_2, \cdots, \chi_n \in A \\ &\chi_{n+1}, \chi_{n+2}, \cdots, \chi_m \in B \end{aligned} \tag{4.16}$$

Then the **H** and **S** matrices are partitioned as follows:

$$\mathbf{H} = \begin{bmatrix} H_A & H_{AB} \\ H_{BA} & H_B \end{bmatrix}$$

$$\mathbf{S} = \begin{bmatrix} S_A & S_{AB} \\ S_{BA} & S_B \end{bmatrix} \qquad (4.17)$$

where the elements of the submatrices are defined as

$$(\mathbf{H}_A)_{ij} = \langle \chi_i | H^{eff} | \chi_j \rangle \qquad \chi_i, \chi_j \in A$$

$$(\mathbf{H}_B)_{ij} = \langle \chi_i | H^{eff} | \chi_j \rangle \qquad \chi_i, \chi_j \in B$$

$$(\mathbf{H}_{AB})_{ij} = (\mathbf{H}_{BA})_{ji} = \langle \chi_i | H^{eff} | \chi_j \rangle \qquad \chi_i \in A, \chi_j \in B$$

$$(\mathbf{S}_A)_{ij} = \langle \chi_i | \chi_j \rangle \qquad \chi_i, \chi_j \in A$$

$$(\mathbf{S}_B)_{ij} = \langle \chi_i | \chi_j \rangle \qquad \chi_i, \chi_j \in B$$

$$(\mathbf{S}_{AB})_{ij} = (\mathbf{S}_{BA})_{ji} = \langle \chi_i | \chi_j \rangle \qquad \chi_i \in A, \chi_j \in B \qquad (4.18)$$

The MO's of the fragments A and B are obtained by the pseudo-eigenvalue equations

$$\mathbf{H}_A \mathbf{C}_A = \mathbf{S}_A \mathbf{C}_A \mathbf{e}_A$$

$$\mathbf{H}_B \mathbf{C}_B = \mathbf{S}_B \mathbf{C}_B \mathbf{e}_B \qquad (4.19)$$

To combine these two equations, we introduce the following matrices:

$$\mathbf{H}^\circ = \begin{bmatrix} \mathbf{H}_A & \mathbf{0} \\ \mathbf{0} & \mathbf{H}_B \end{bmatrix}$$

$$\mathbf{S}^\circ = \begin{bmatrix} \mathbf{S}_A & \mathbf{0} \\ \mathbf{0} & \mathbf{S}_B \end{bmatrix}$$

$$\mathbf{C}^\circ = \begin{bmatrix} \mathbf{C}_A & \mathbf{0} \\ \mathbf{0} & \mathbf{C}_B \end{bmatrix}$$

$$\mathbf{e}^\circ = \begin{bmatrix} \mathbf{e}_A & \mathbf{0} \\ \mathbf{0} & \mathbf{e}_B \end{bmatrix} \qquad (4.20)$$

These matrices satisfy the following pseudo-eigenvalue equation

$$\mathbf{H}^\circ \mathbf{C}^\circ = \mathbf{S}^\circ \mathbf{C}^\circ \mathbf{e}^\circ, \qquad (4.21)$$

which is equivalent to Eq. 4.19. Thus the FMO's ψ_i^0 can be re-written as

$$\psi_i^0 = \sum_\mu C_{\mu i}^0 \chi_\mu \tag{4.22}$$

The FMO ψ_i^0 belongs to fragment A if $1 \le i \le n$, and to fragment B if $n+1 \le i \le m$.

The MO's ψ_i of a molecule is expressed in terms of its FMO's as

$$\psi_i = \sum_j T_{ji} \psi_j^0 \tag{4.23}$$

where T_{ji} is the coefficient for the FMO ψ_j^0 in the MO ψ_i. The T_{ji} coefficients form the m x m matrix **T**. This matrix relates the **C** and $\mathbf{C}^\circ$ matrices as

$$\mathbf{C} = \mathbf{C}^\circ \mathbf{T} \tag{4.24}$$

and is given by

$$\mathbf{T} = (\mathbf{C}^\circ)^\dagger \mathbf{S}^\circ \mathbf{C} \tag{4.25}$$

The overlap $\tilde{S}_{ij}$ and the interaction energy $\tilde{H}_{ij}$ between the FMO ψ_i^0 of fragment A and the FMO ψ_j^0 of fragment B are given by

$$\tilde{S}_{ij} = \left\langle \psi_i^0 \middle| \psi_j^0 \right\rangle = (\mathbf{C}_i^0)^\dagger \mathbf{S}\, \mathbf{C}_j^0$$

$$\tilde{H}_{ij} = \left\langle \psi_i^0 \middle| H^{eff} \middle| \psi_j^0 \right\rangle = (\mathbf{C}_i^0)^\dagger \mathbf{H}\, \mathbf{C}_j^0 \tag{4.26}$$

where $\mathbf{C}_j^0$ is the column vector made up of the MO coefficients $C_{\mu j}$, and $(\mathbf{C}_i^0)^\dagger$ is the row vector made up of the MO coefficients $C_{\mu i}$.

4.2.4 Density of states

Electronic structure of simple molecular systems are easy to describe in terms of the nodal properties and energies of their MO's. For large, complex molecular systems this approach is intractable and hence useless. To discuss the electronic structures of such systems it is convenient to use the concepts of density of states (DOS), projected DOS (PDOS), and "density of overlap populations" (DOP) in analogy with electronic band structure description for solids.[4,5]

The DOS, n(e), refers to the number of the energy levels lying between e and e + de, where de is a small positive number. That is, n(e) is the probability of the energy level at e. The MO levels allowed for any molecular system are discrete so that its DOS curve, i.e., the n(e)-vs.-e plot, is difficult to visualize. To overcome this difficulty, each discrete MO level may be replaced with a Gaussian function centered at the energy level. For example, consider an MO level e_i with the probability of occurrence p_i (= 1 for each nondegenerate MO level) (*Figure 4.3a*). This discrete level at e_i may be replaced by the Gaussian function $g_i(e)$ centered at e_i as shown in *Figure 4.3b*, so that

$$g_i(e) = \frac{1}{\sqrt{\pi}\delta} p_i \exp\left[-\left(\frac{e - e_i}{\delta}\right)^2\right] \tag{4.27}$$

where δ is the smoothing parameter. The function $g_i(e)$ becomes flatter with increasing δ, and satisfies the normalization condition

$$\int_{-\infty}^{\infty} g_i(e)de = p_i \tag{4.28}$$

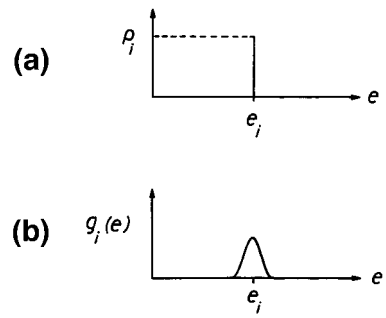

Figure 4.3. (a) Discrete energy level e_i with probability p_i. (b) Representation of the discrete level in terms of the Gaussian function $g_i(e)$.

The DOS, n(e), at any given energy e is then obtained by summing contributions from the Gaussian functions $g_i(e)$ for all the MO levels i = 1, 2, ⋯, m,

$$n(e) = \sum_{i=1}^{m} 2g_i(e) \tag{4.29}$$

where the factor of 2 is introduced because each level can be occupied by two electrons. In other words, we neglect high-spin states, for which some levels are singly filled (see *Section 4.6.1*).

Suppose that we calculate the gross population $q_\mu(e_i)$ of an atomic orbital χ_μ for each individual MO level e_i alone assuming that it is doubly occupied. Then the DOS-weighted gross population, $q_\mu(e)$, of the orbital χ_μ is given as

$$q_\mu(e) = \sum_i g_i(e) q_\mu(e_i) \tag{4.30}$$

Then $q_\mu(e)$ represents the PDOS of the atom orbital χ_μ. The PDOS, $Q_A(e)$, of an atom A is given by

$$Q_A(e) = \sum_{\chi_\mu \in A} q_\mu(e), \tag{4.31}$$

which satisfies the normalization condition

$$n(e) = \sum_{all\ A} Q_A(e) \tag{4.32}$$

The gross population Q_A of atom A is then written as

$$Q_A = \int_{-\infty}^{e_f} Q_A(e)de, \tag{4.33}$$

where e_f refers to the HOMO level.

In a similar manner, the overlap population $p_{\mu\nu}(e_i)$ between two atomic orbitals χ_μ and χ_ν can be calculated for each individual MO level e_i alone assuming that it is doubly occupied. Then the DOS-weighted overlap population $p_{\mu\nu}(e)$ between orbitals χ_μ and χ_ν is given by

$$p_{\mu\nu}(e) = \sum_i g_i(e)p_{\mu\nu}(e_i), \tag{4.34}$$

which represents the DOP between orbitals χ_μ and χ_ν. The DOP, $p_{AB}(e)$, between atoms A and B is given by

$$p_{AB}(e) = \sum_{\chi_\mu \in A} \sum_{\chi_\nu \in A} p_{\mu\nu}(e) \tag{4.35}$$

and the overlap population P_{AB} between atoms A and B is written as

$$P_{AB} = \int_{-\infty}^{e_f} p_{AB}(e)de \tag{4.36}$$

Electronic structures of molecules can be discussed solely on the basis of their DOS and or DOP values. This approach totally neglects the information about the nodal properties of MO's. However, consequences of orbital interactions leading to calculated MO levels can be easily deciphered by constructing appropriate DOS, PDOS and DOP plots.

4.3 EHTB calculations [6]

The crucial difference between first principles and semi-empirical methods of electronic structure calculations lies in the way of constructing the **H** matrix of the pseudo-eigenvalue equation Eqs. 4.8. Once a set of basis atomic orbitals is chosen for a system under consideration, first principles methods construct the **H** matrix using the Hamiltonian appropriate for the system and refine it in a self consistent field manner. In semi-empirical methods, the construction of **H** is carried out empirically by introducing a number of simplifying approximations.

In the EHTB method,[6] only valence electrons are considered, and valence atomic orbitals are approximated by Slater type orbitals (STO's) χ_μ. Single-zeta STO's are defined by

$$\chi_\mu(r,\theta,\phi) \propto r^{n-1} \exp(-\zeta r)\, Y(\theta,\phi) \tag{4.37}$$

where n is the principal quantum number, ζ is the exponent, and $Y(\theta, \phi)$ is the spherical harmonics. In double-zeta STO's, a linear combination of two exponential functions is used as

$$\chi_\mu(r,\theta,\phi) \propto$$

$$r^{n-1} [c_1 \exp(-\zeta_1 r) + c_2 \exp(-\zeta_2 r)] Y(\theta,\phi) \qquad (4.38)$$

The values of ζ for single-zeta STO's, and those of ζ_1, ζ_2, c_1 and c_2 for double-zeta STO's, can be taken from results of atomic electronic structure calculations using the Hartree-Fock method.[7] These calculations do not provide information about unoccupied valence atomic orbital(s) of an atom (e.g., 2p orbital of Li, 4p orbitals of Ti, etc.).

In the EHTB method the exact mathematical forms of the effective Hamiltonian H^{eff} is not specified. Instead, the matrix representation of H^{eff} is empirically constructed. The diagonal element $H_{\mu\mu} = \langle\chi_\mu|H^{eff}|\chi_\mu\rangle$ (μ = 1, 2, ···, m) is approximated by the valence-state ionization potential (VSIP),[8,9]

$$H_{\mu\mu} = -\text{VSIP} \qquad (4.39)$$

The VSIP values of valence atomic orbitals can be approximated by their orbital energies from suitable atomic electronic structure calculations.[7]

The off-diagonal matrix element between orbitals χ_μ and χ_ν, i.e., $H_{\mu\nu} = \langle\chi_\mu|H^{eff}|\chi_\nu\rangle$, is approximated by the Wolfsberg-Helmholz formula,[8]

$$H_{\mu\nu} = KS_{\mu\nu}(H_{\mu\mu} + H_{\nu\nu})/2 \qquad (4.40)$$

where $S_{\mu\nu}$ is the overlap integral between χ_μ and χ_ν, $S_{\mu\nu} = \langle\chi_\mu|\chi_\nu\rangle$, K is a constant (i.e., 1.75), and $H_{\mu\mu}$ and $H_{\nu\nu}$ are the VSIP's of the orbitals χ_μ and χ_ν, respectively. In the weighted Wolfsberg-Helmholz approximation,[10] the constant K is replaced with another constant K'

$$K' = K + \Delta^2 + \Delta^4(1 - K) \qquad (4.41)$$

where $\Delta = (H_{\mu\mu} - H_{\nu\nu})/(H_{\mu\mu} + H_{\nu\nu})$. The weighted Wolfsberg-Helmholz formula reduces the extent of the so-called counterintuitive orbital mixing that occurs when a very contracted orbital interact with a very diffuse orbital.[10]

The EHTB method solves Eq. 4.8 for molecules using the matrix elements defined as above. The simple Hückel method solves Eq. 4.9. The ζ and $H_{\mu\mu}$ values of the STO's to be used in constructing the **H** and **S** matrices are stored in the data base of the *CAESAR* program package (see *Section 5.2.2* for details).

4.4 Electronic structures of solids [9,10]

4.4.1 Bloch orbitals

Consider a 3D orthorhombic lattice with repeat distances *a*, *b* and *c* along the crystallographic a-, b- and c-direction, respectively, as shown in *Figure 4.4a*. Each unit cell has a set of atomic orbitals $\{\chi_1, \chi_2, \cdots, \chi_m\}$. An atomic orbital χ_μ (μ = 1, 2, ···, m) in the unit cell located at the site (m*a*, n*b*, p*c*) is written as χ_μ(**r**-m**a**-n**b**-p**c**), where m, n and p are integers. To determine the electronic energy bands arising from such atomic orbitals, one first defines the Bloch orbitals ϕ_μ for each atomic orbital χ_μ as

$\phi_\mu(k_a,k_b,k_c) =$

$$N^{-1/2}\sum_n \exp(ik_a ma)\exp(ik_b nb)\exp(ik_c pc)\chi_\mu(\mathbf{r}\text{-m}\mathbf{a}\text{-n}\mathbf{b}\text{-p}\mathbf{c}) \qquad (4.42)$$

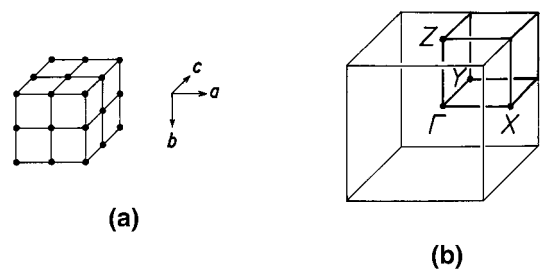

Figure 4.4. (a) Schematic representation of the direct lattice sites generated by the repeat vectors a, b and c. (b) Schematic diagram of the FPZ, where G = (0, 0, 0), X = (1/2, 0, 0), Y = (0, 1/2, 0), and Z = (0, 0, 1/2).

Here the three wave vectors k_a, k_b and k_c are used to describe all possible phase relationships between the atomic orbitals located at different unit cells along the *a*-, *b*- and *c*- directions, respectively. Due to the periodic nature of the coefficients $\exp(ik_a ma)$, $\exp(ik_b nb)$ and $\exp(ik_c pc)$, one can use only the wave vectors (k_a, k_b, k_c) lying in the following region

$$\begin{aligned} -\pi/a &\le k_a \le \pi/a \\ -\pi/b &\le k_b \le \pi/b \\ -\pi/c &\le k_c \le \pi/c \end{aligned} \qquad (4.43)$$

in constructing the Bloch orbitals. These wave vectors define the first primitive zone (FPZ) shown in *Figure 4.4b*, where Γ = (0, 0, 0), X = (π/a, 0, 0), Y = (0, π/b, 0) and Z = (0, 0, π/c).

4.4.2 First primitive zone

In describing electronic band structures of general 3D solids, the concepts of the direct and reciprocal lattices are employed. For a 3D lattice with repeat vectors **a**, **b** and **c**, the positions of lattice sites (m*a*, n*b*, p*c*) are represented as vectors **R**,

$$\mathbf{R} = m\mathbf{a} + n\mathbf{b} + p\mathbf{c} \qquad (4.44)$$

A set of these vectors is called the direct lattice. The reciprocal lattice of a given direct lattice is defined as a set of vectors **K** satisfying the relationship, exp (**K**•**R**) = l. The vectors **K** are expressed as

$$\mathbf{K} = m\mathbf{a}^* + n\mathbf{b}^* + p\mathbf{c}^* \qquad (4.45)$$

where **a***, **b*** and **c*** are the reciprocal vectors associated with the vectors **a**, **b** and **c** as follows:

$$\mathbf{a}^* = 2\pi \frac{\mathbf{b} \times \mathbf{c}}{V}$$

$$\mathbf{b}^* = 2\pi \frac{\mathbf{c} \times \mathbf{a}}{V} \qquad (4.46)$$

$$\mathbf{c}^* = 2\pi \frac{\mathbf{a} \times \mathbf{b}}{V}$$

where V is the volume of the unit cell defined by the repeat vectors **a**, **b** and **c** (i.e., V = **a**×**b**·**c**). Thus, for the orthorhombic lattice, the lengths of **a***, **b*** and **c*** are given by $2\pi/a$, $2\pi/b$ and $2\pi/c$, respectively, and their directions are along **a**, **b** and **c**, respectively.

It is convenient to express a general position, **k**, of the reciprocal space in units of the reciprocal vectors, that is,

$$\mathbf{k} = x\mathbf{a}^* + y\mathbf{b}^* + z\mathbf{c}^* \qquad (4.47)$$

where x, y and z are dimensionless numbers. For any general 3D lattice, the term exp(i**k**•**R**) can be written as

$$\exp(i\mathbf{k}\bullet\mathbf{R}) = \exp(ik_a m a)\exp(ik_b n b)\exp(ik_c p c) \qquad (4.48)$$

where $k_a = x(2\pi/a)$, $k_b = y(2\pi/b)$ and $k_c = z(2\pi/c)$. Therefore, the wave vectors (k_a, k_b, k_c) introduced to construct the Bloch orbitals of a 3D orthorhombic lattice are also valid for any other non-orthorhombic lattice.

For simplicity, the wave vector **k** = (xa*, yb*, zc*) is often represented by (x, y, z). With this notation, the special points of the FPZ in *Figure 4.4b* is given by Γ = (0, 0, 0), X = (0.5, 0, 0), Y = (0, 0.5, 0) and Z = (0, 0, 0.5). Likewise, the FPZ of the reciprocal space is defined by

$$\begin{aligned} -0.5 &\le x \le 0.5 \\ -0.5 &\le y \le 0.5 \\ -0.5 &\le z \le 0.5 \end{aligned} \qquad (4.49)$$

The first Brillouin zone (FBZ) is defined as the Wigner-Seitz cell of a reciprocal space. For an orthorhombic lattice, the FPZ is identical with the FBZ. This is not necessarily the case for other lattices. One can use wave vectors of either FPZ or FBZ in constructing electronic band structures.

4.4.3 Crystal orbitals

Our notations for Bloch orbitals and their related expressions are considerably simplified by using the symbols **k** and **R**. An atomic orbital χ_μ located at **R** is given by $\chi_\mu(\mathbf{r}\text{-}\mathbf{R})$ (μ = 1, 2, ···, m), so the Bloch orbital ϕ_μ is written as

$$\phi_\mu(\mathbf{k}) = N^{-1/2} \sum_{\mathbf{R}} \exp(i\mathbf{k}\bullet\mathbf{R})\chi_\mu(\mathbf{r}\text{-}\mathbf{R}) \qquad (4.50)$$

The crystal orbitals ψ_i are given as linear combinations of the Bloch orbitals ϕ_μ

$$\psi_i(\mathbf{k}) = \sum_{\mu} C_{\mu i}(\mathbf{k})\phi_\mu(\mathbf{k}) \tag{4.51}$$

and their energies $e_i(\mathbf{k})$ are eigenvalues associated with the effective Hamiltonian H^{eff}

$$H^{eff}\ \psi_i(\mathbf{k}) = e_i(\mathbf{k})\ \psi_i(\mathbf{k}) \tag{4.52}$$

so the energy $e_i(\mathbf{k})$ is written as

$$e_i(\mathbf{k}) = \frac{\langle \psi_i(\mathbf{k}) | H^{eff} | \psi_i(\mathbf{k}) \rangle}{\langle \psi_i(\mathbf{k}) | \psi_i(\mathbf{k}) \rangle} \tag{4.53}$$

The energy $e_i(\mathbf{k})$ is optimum with respect to changes in coefficients $C_{\kappa i}(\mathbf{k})$, i.e.,

$$\frac{\partial e_i(\mathbf{k})}{\partial C_{\kappa i}(\mathbf{k})} = 0 \qquad (\kappa = 1, 2, \cdots, m) \tag{4.54}$$

which leads to the m x m secular determinant

$$\begin{vmatrix} H_{11}(\mathbf{k}) - e_i(\mathbf{k})S_{11}(\mathbf{k}) & H_{12}(\mathbf{k}) - e_i(\mathbf{k})S_{12}(\mathbf{k}) & \bullet\ \bullet & H_{1m}(\mathbf{k}) - e_i(\mathbf{k})S_{1m}(k) \\ H_{21}(\mathbf{k}) - e_i(\mathbf{k})S_{21}(\mathbf{k}) & H_{22}(\mathbf{k}) - e_i(\mathbf{k})S_{22}(\mathbf{k}) & \bullet\ \bullet & H_{2m}(\mathbf{k}) - e_i(\mathbf{k})S_{2m}(k) \\ \bullet & \bullet & \bullet\ \bullet & \bullet \\ \bullet & \bullet & \bullet\ \bullet & \bullet \\ H_{m1}(\mathbf{k}) - e_i(\mathbf{k})S_{m1}(\mathbf{k}) & H_{m2}(\mathbf{k}) - e_i(\mathbf{k})S_{m2}(\mathbf{k}) & \bullet\ \bullet & H_{mm}(\mathbf{k}) - e_i(\mathbf{k})S_{mm}(\mathbf{k}) \end{vmatrix} = 0 \tag{4.55}$$

where the matrix elements $H_{\mu\nu}(\mathbf{k})$ and $S_{\mu\nu}(\mathbf{k})$ are expressed as

$$H_{\mu\nu}(\mathbf{k}) = \langle\phi_\mu(\mathbf{k})|H^{eff}|\phi_\nu(\mathbf{k})\rangle = \langle\chi_\mu(\mathbf{r})|H^{eff}|\chi_\nu(\mathbf{r})\rangle$$
$$+ \sum_{\mathbf{R}} \{\exp(-i\mathbf{k}\cdot\mathbf{R})\langle \chi_\mu(\mathbf{r}-\mathbf{R}) | H^{eff} | \chi_\nu(\mathbf{r}) \rangle$$
$$+ \exp(i\mathbf{k}\cdot\mathbf{R})\langle \chi_\mu(\mathbf{r}) | H^{eff} | \chi_\nu(\mathbf{r}-\mathbf{R}) \rangle\} \tag{4.56}$$

$$S_{\mu\nu}(\mathbf{k}) = \langle\phi_\mu(\mathbf{k})|\phi_\nu(\mathbf{k})\rangle = \langle\chi_\mu(\mathbf{r})|\chi_\nu(\mathbf{r})\rangle$$
$$+ \sum_{\mathbf{R}} \{\exp(-i\mathbf{k}\cdot\mathbf{R})\langle \chi_\mu(\mathbf{r}-\mathbf{R}) | \chi_\nu(\mathbf{r}) \rangle$$
$$+ \exp(i\mathbf{k}\cdot\mathbf{R})\langle \chi_\mu(\mathbf{r}) | \chi_\nu(\mathbf{r}-\mathbf{R}) \rangle\} \tag{4.57}$$

The summations of Eqs. 4.56 and 4.57 are known as lattice sums. The summations start from the reference unit cell at **R** = 0 and go over the neighboring unit cells located at **R** (≠ 0). The matrix elements $\langle \chi_\mu(\mathbf{r}) | H^{eff} | \chi_\nu(\mathbf{r} - \mathbf{R}) \rangle$ and $\langle \chi_\mu(\mathbf{r}) | \chi_\nu(\mathbf{r} - \mathbf{R}) \rangle$ become smaller with increasing the distance between the reference and the neighbor cells. Eventually, they become negligible beyond a certain value $\mathbf{R}_0 = n_a\mathbf{a} + n_b\mathbf{b} + n_c\mathbf{c}$, where n_a, n_b and n_c are the n-th nearest neighbors along the a- b- and c-directions, respectively. Thus the lattice sums can be truncated by dropping terms associated with the unit cells beyond $\mathbf{R}_0$.

For a unit cell containing m atomic orbitals $\{\chi_1, \chi_2, \cdots, \chi_m\}$, the matrix elements $H_{\mu\nu}(\mathbf{k})$, $S_{\mu\nu}(\mathbf{k})$ and $C_{\mu i}(\mathbf{k})$ (μ, ν, i = 1, 2, ···, m) form m x m matrices **H**(**k**), **S**(**k**) and **C**(**k**), respectively. These matrices are related by the pseudo-eigenvalue equation,

$$\mathbf{H}(\mathbf{k})\,\mathbf{C}(\mathbf{k}) = \mathbf{S}(\mathbf{k})\,\mathbf{C}(\mathbf{k})\,\mathbf{e}(\mathbf{k}) \qquad (4.58)$$

where **e**(**k**) is an m x m diagonal matrix with its diagonal elements given by $e_i(\mathbf{k})$ (i = 1, ···, m). Thus if the matrices **H**(**k**) and **S**(**k**) are determined, then the crystal orbitals **C**(**k**) and orbital energies **e**(**k**) are found by solving the pseudo-eigenvalue problem, Eq. 4.58. If the overlap matrix **S**(**k**) is approximated by the unit matrix **1**, then Eq. 4.58 is simplified as

$$\mathbf{H}(\mathbf{k})\,\mathbf{C}(\mathbf{k}) = \mathbf{C}(\mathbf{k})\,\mathbf{e}(\mathbf{k}) \qquad (4.59)$$

4.5 Describing electronic structures of solids

4.5.1 Dispersion relations

A study of the electronic band structure of a given solid requires solving Eq. 4.58 for a set of k-points. To obtain a dispersion relation for a band $\psi_i(\mathbf{k})$ along a specific line segment of the FPZ, one needs to calculate its energy $e_i(\mathbf{k})$ at a number of k-points covering that direction. This is illustrated in *Figure 4.5a* for a band of a 1D system, where the circles refer to the calculated energies at chosen k-values. The dispersion relation is then obtained by connecting those calculated energy values (solid line in *Figure 4.5a*). Typically dispersion relations are plotted along the boundaries of the FPZ. For the FPZ of a 3D lattice, the special points of interest are

$$\begin{aligned}
&\Gamma = (0, 0, 0)\\
&X = (0.5, 0, 0)\\
&Y = (0, 0.5, 0)\\
&Z = (0, 0, 0.5)\\
&XY = (0.5, 0.5, 0)\\
&XZ = (0.5, 0, 0.5)\\
&YZ = (0, 0.5, 0.5)\\
&XYZ = (0.5, 0.5, 0.5)
\end{aligned} \qquad (4.60)$$

and dispersion relations can be drawn between any two points. For the purpose of labeling in dispersion plots, simpler labels are needed for the XY, XZ, YZ and XYZ points. In this book and the *CAESAR* package, the following notations are adopted: M = XY, N = XZ, L = YZ, and R = XYZ.

A complicated situation arises when two bands overlap in energy as shown in *Figure 4.5b*. If the symmetries of the two band levels differ at all k-points along Γ→X, the two band dispersion curves cross as indicated in *Figure 4.5b*. However, if the two bands have an identical symmetry along Γ→X, crossing of the dispersion curves is not possible so that there result in two narrower bands as illustrated in *Figure 4.5c*. To determine which is correct, one may either analyze the symmetry of the crystal orbitals describing the two bands or calculate the $e_i(k)$ values for a fine mesh of k-points in the vicinity of the crossing (or intended crossing) point. Even when band dispersions cross as in *Figure*

4.5b, it is important to notice the meaning of an energy band from the viewpoint of energy surface as a function of wave vector; the lower energy surface (i.e., that lying below the crossing point) of *Figure 4.5b* is one band, and the upper surface (i.e., that lying above the crossing point) is another. This classification is important in understanding Fermi surfaces of partially filled bands (see later).

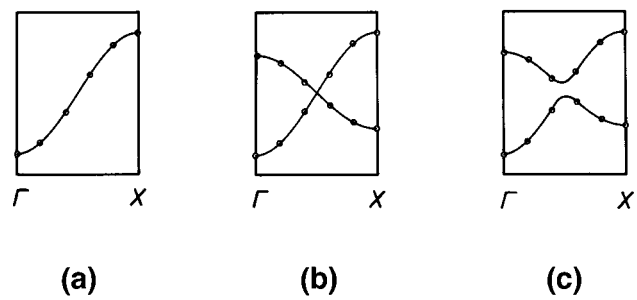

Figure 4.5. Determination of band dispersion relations along the line segment G-X for the cases of (a) one band, (b) two bands with crossing, (c) two bands with avoided crossing.

4.5.2 Fermi level and k-point sets

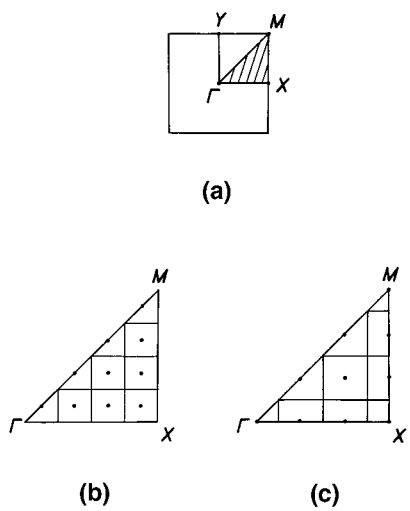

Figure 4.6. FPZ of a square lattice. (a) One whole FPZ. A set of wave vectors lying in the shaded triangle can be used to sample the wave vectors of the whole FPZ. (b) Uniform distribution of k-points excluding the borders of the FPZ. (c) Uniform distribution of k-points including the borders of the FPZ.

We now discuss how the Fermi level (here used to mean the highest occupied energy level) can be determined by considering a 2D square lattice, for which the FPZ is a square in reciprocal space. To know the dependence of $e_i(\mathbf{k})$ and $\psi_i(\mathbf{k})$ on the wave vectors **k** of the FPZ, it is necessary to calculate them for a set of k-points evenly distributed in the FPZ. Because of the symmetry $e_i(\mathbf{k}) = e_i(-\mathbf{k})$, it is sufficient to use a set of k-points covering half the FPZ. Depending on the symmetry of the FPZ, a set of k-points can be chosen from a smaller part of half the FPZ. For example, in *Figure 4.6a*, only the

wave vectors in the shaded triangle are necessary to consider. To examine the $e_i(k)$-versus-k relationship for the k values of the shaded triangle, a set of L points $\{k_1, k_2, \cdots, k_L\}$ may be evenly distributed to cover the shaded triangle. For example, *Figures 4.6b* and *4.6c* show two ways of distributing a set of 10 k-points. The k-points avoid the boundary lines in *Figure 4.6b*, while this is not the case in *Figure 4.6c*. In a set of evenly distributed k-points, each k-point represents all the k-values in the small square surrounding that point, because in reciprocal space all k-points are equally allowed. Depending upon where the k-point lies, it may represent only a fraction of the little square. For instance, each k-point of *Figure 4.6b* lying on the $\Gamma \rightarrow M$ line represents half the little square. In general, it is necessary to define the weight W_i of each $\mathbf{k}_i$ points such that W_i is proportional to the area $\mathbf{k}_i$ represents and satisfies the normalization condition

$$\sum_{i=1}^{L} W_i = 1 \qquad (4.61)$$

Thus, in *Figure 4.6c*, the weights of the k-points (0, 0), (1/2, 0), (1/3, 0), and (1/3, 1/6) have the ratios 1/8 : 1/4 : 1/2 : 1.

When the crystal orbitals $\psi_n(\mathbf{k})$ are generated using a set of atomic orbitals $\{\chi_1, \chi_2, \cdots, \chi_m\}$ per unit cell, one obtains a set of m orbital energies $\{e_1(\mathbf{k}_i), e_2(\mathbf{k}_i), \cdots, e_m(\mathbf{k}_i)\}$ for each $\mathbf{k}_i$ point. Each band level $e_n(\mathbf{k}_i)$ has its probability of occurrence $p_n(\mathbf{k}_i)$, which is the same as the weight W_i of the k-point $\mathbf{k}_i$. Thus, there are a set of probabilities $\{p_1(\mathbf{k}_i), p_2(\mathbf{k}_i), \cdots, p_m(\mathbf{k}_i)\}$ to consider for each $\mathbf{k}_i$ point, where

$$p_n(\mathbf{k}_i) = W_i \qquad (n = 1, 2, \cdots, m) \qquad (4.62)$$

The probability $p_n(\mathbf{k}_i)$ has the meaning that a doubly occupied crystal orbital $\psi_n(\mathbf{k}_i)$ accounts for $2p_n(\mathbf{k}_i)$ electrons. If electronic band structure calculations are performed for the L points of a set $\{\mathbf{k}_1, \mathbf{k}_2, \cdots, \mathbf{k}_L\}$, one obtains m x L band levels and their probabilities

$$\{e_1(\mathbf{k}_i), e_2(\mathbf{k}_i), \cdots, e_m(\mathbf{k}_i)\} \ (i = 1, 2, \cdots, L) \qquad (4.63)$$

$$\{p_1(\mathbf{k}_i), p_2(\mathbf{k}_i), \cdots, p_m(\mathbf{k}_i)\} \ (i = 1, 2, \cdots, L) \qquad (4.64)$$

The m x L band levels of Eq. 4.63 may now be rearranged in ascending order of energy. This ordered set of m x L levels can be simply written as

$$\{e_1, e_2, \cdots, e_m, e_{m+1}, \cdots, e_{2m}, \cdots, e_{mxL}\} \qquad (4.65)$$

The m x L probabilities of Eq. 4.64 can also be arranged as in the orbital energy sequence of Eq. 4.63 to give the ordered set of m x L probabilities, which may be written as

$$\{p_1, p_2, \cdots, p_m, p_{m+1}, \cdots, p_{2m}, \cdots, p_{mxL}\} \qquad (4.66)$$

As already mentioned, each doubly occupied level e_i of Eq. 4.65 accounts for $2p_i$ electrons. Therefore for any number of electrons N per unit cell, one can find the energy levels e_{max} and e_{max+1} satisfying the constraint

$$\sum_{i=1}^{max} 2p_i \le N < \sum_{i=1}^{max+1} 2p_i \qquad (4.67)$$

In considering the Fermi level e_f, it is important to consider the e_{max} and e_{max+1} values for the case when N refers to the total number of electrons, N_{elec}, in a unit cell. Then e_{max} and e_{max+1} are the highest occupied and lowest unoccupied levels, respectively. Thus, for normal semiconductors and insulators, the energy difference $e_{max+1} - e_{max}$ is the band gap. For normal metals, this energy difference should be zero in principle, but may be nonzero in practice because a set of finite k-points is used in sampling the FPZ. In a special case like a single graphite sheet, the Fermi surface consists of only one k-point, i.e., K = (1/3, 1/3). The FPZ of the 2D graphite lattice is given by a rhombus so that when this FPZ is sampled by a set of evenly distributed k-points, the point (1/3, 1/3) is not included in the set. Therefore, the energy difference $e_{max+1} - e_{max}$ will be nonzero. In this case, the true Fermi level can be approximated by $e_f = (e_{max+1} + e_{max})/2$ if the k-point set employed did not include the K point. To be precise, one should carry out calculations for the K point.

For convenience, the highest occupied level of a given system determined as described above is defined as the Fermi level e_f of the system. However, it should be recalled that the double occupancy of each band level is assumed in obtaining this level. Therefore, this level is not relevant for discussing the highest occupied level of magnetic insulators, for which one must consider the single occupancy of all band levels for some bands (see *Section 4.6.1*).[2]

4.5.3 Density of states

When the electronic band structure of a solid is calculated for a fine mesh of **k**-points covering the FPZ, one obtains a set of m×L discrete energy levels and their probabilities of occurrence (Eqs. 4.65 and 4.66). Then, as described in *Section 4.2.4*, the DOS n(e) at a given energy e can be obtained by summing contributions from the Gaussian functions $g_i(e)$ that represent for all the m×L levels,

$$n(e) = \sum_{i=1}^{m\times L} 2g_i(e) \qquad (4.68)$$

where the factor of 2 is introduced because each level can be occupied by two electrons. (We neglect the possibility of electron localization, which in a one-electron band picture is represented by singly filled band levels. See *Section 4.6.1*.) The smoothing parameter δ of $g_i(e)$ (see Eq. 4.27) is chosen according to the size of the k-points mesh. The accuracy of n(e) is improved by using a small value of δ with a large set of k-points.

n(e) means the probability of the energy level at e, so that it is nonzero within the allowed energy region of a band and vanishes in the forbidden energy region. An important DOS value in describing the physical properties of metals is the DOS value at the Fermi level, i.e., $n(e_f)$. In terms of n(e), the electronic energy E_{elec} of a system is written as

$$E_{elec} = \int_{-\infty}^{e_f} n(e)\, e\, de \qquad (4.69)$$

A band of nonmagnetic systems can accommodate two electrons per unit cell so the DOS values of a given band i, $n_i(e)$, satisfy the normalization condition

$$\int_{-\infty}^{\infty} n_i(e)de = 2 \qquad (4.70)$$

Suppose that we calculate the gross population $q_\mu(e_i)$ of an atomic orbital χ_μ as well as the overlap population $p_{\mu\nu}(e_i)$ between two atomic orbitals χ_μ and χ_ν for each individual level e_i assuming that it is doubly occupied. Then the PDOS $q_\mu(e)$ of orbital χ_μ, the PDOS $Q_A(e)$ of atom A,

the PDOP $p_{\mu\nu}(e)$ for orbitals χ_μ and χ_ν, and the PDOP $p_{AB}(e)$ for the bond between atoms A and B are defined as described in *Section 4.2.4*. The PDOP plots for solids are known as crystal orbital overlap population (COOP) curves.[4]

Electronic band structure calculations for a solid generate a large number (i.e., m×L) of levels. Thus as in the case for large, complex molecules, it is practical to use appropriate DOS, PDOS and DOP plots in describing electronic structures of solids.

4.6 Partially filled bands

From the viewpoint of one-electron band theory, a system with partially filled band(s) is metallic. However, it should be recalled that such a system can be a magnetic insulator due to electron-electron repulsion. Normal metals and magnetic insulators are similar in that they both possess partially filled energy levels. Whether a system with partially filled band(s) is metallic or magnetic insulating depends on how the partially filled bands are occupied.[2]

4.6.1 Normal metallic versus magnetic insulating states of a partially filled band

To examine what controls the relative energies of metallic and magnetic insulating states of a partially filled band system, we consider a hypothetical 1D chain with one orbital χ_i and one electron on each lattice site i (*Figure 4.7a*).[2,12] The energy factors governing the relative energies of the two states of this chain are similar to those that govern the relative energies of the high-spin and low-spin states of a molecular dimer (*Figure 4.8a*). The molecular orbitals of the dimer can be approximated by

$$\psi_1 = \frac{\chi_1 + \chi_2}{\sqrt{2}}$$

$$\psi_2 = \frac{\chi_1 - \chi_2}{\sqrt{2}} \qquad (4.71)$$

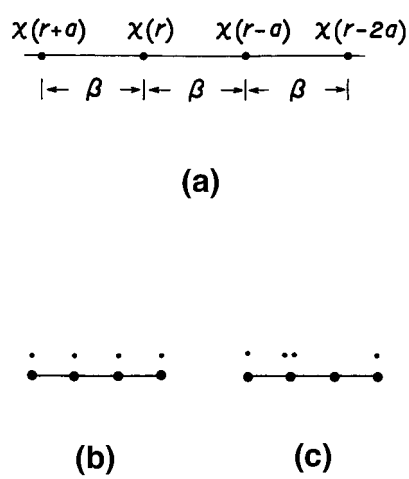

Figure 4.7. (a) 1D lattice with one orbital and one electron per site. (b) Magnetic insulating state of a 1D chain with one electron per site, in which an electron is localized at each site. (c) Intermediate stage of the electron transport process in a 1D chain with one electron per site.

if the overlap integral $<\chi_1|\chi_2>$ is neglected. Then, the energies of these orbitals are given by $e_1 = \alpha + \beta$ and $e_2 = \alpha - \beta$, where $\beta = <\chi_1|H^{eff}|\chi_2>$. With two electrons, one may construct the low-spin state (*Figure 4.8b*) or the high-spin state (*Figure 4.8c*). In a one-electron picture, in which electron-electron repulsion is neglected, the low-spin state is always more stable than the high-spin state. This is not necessarily the case when electron-electron repulsion is taken into consideration.

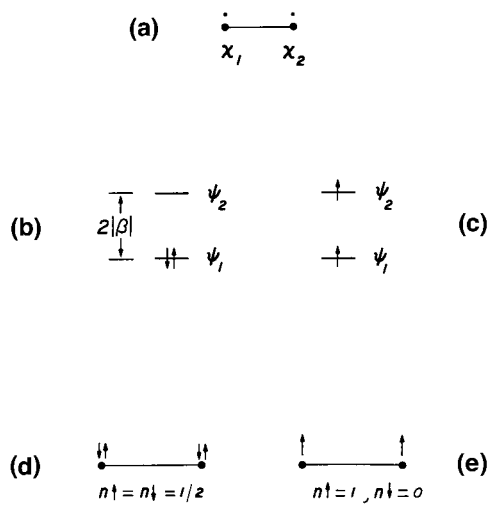

Figure 4.8. (a) Dimer with one orbital and one electron per site. (b) Electron configuration in the low-spin state of the dimer. (c) Electron configuration in the high-spin state. (d) On-site electron density distribution in the low-spin state. (e) On-site electron density distribution in the high-spin state.

To simplify our discussion, we neglect all repulsion integrals but the on-site repulsion $U = (\chi_1\chi_1|\chi_1\chi_1) = (\chi_2\chi_2|\chi_2\chi_2)$. Then, in any electronic state, an atomic site with the up-spin and down-spin electron densities $n\uparrow$ and $n\downarrow$, respectively, contributes the amount of repulsion given by $n\uparrow n\downarrow U$. The on-site charge densities associated with the low-spin (*Figure 4.8b*) and high-spin (*Figure 4.8c*) states are depicted in *Figures 4.8d* and *4.8e*, respectively. In terms of the on-site repulsion, the low-spin state is less stable than the high-spin state by U/2. In terms of the orbital energies, however, the low-spin state is more stable than the high-spin state by $2|\beta|$, which is equal to W/2, where W is the bandwidth of the corresponding 1D chain (*Figure 4.7a*). Consequently, the high-spin state becomes more stable if $U > W$.[2]

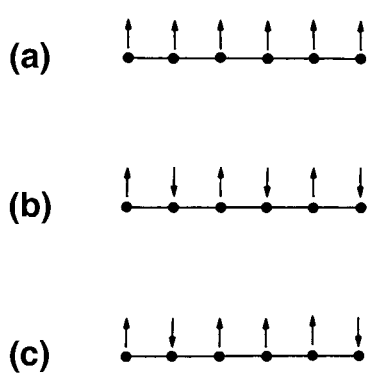

Figure 4.9. Arrangements of localized spins in a 1D chain with one electron per site: (a) Ferromagnetic arrangement, (b) antiferromagnetic arrangement. (c) No long-range order.

Consider the 1D lattice in *Figure 4.7a*. When U >> W, favorable electronic states are those in which each site has one electron with either up or down spin (*Figure 4.7b*). All these states are insulating in nature, because electron hopping from one site to another leads to a situation in which two electrons reside on a single site thereby causing on-site repulsion (*Figure 4.7c*). Such insulating states resulting from partially filled bands are referred to as Mott-Hubbard localized states.[12] *Figures 4.9a* and *4.9b* represent ferromagnetic and antiferromagnetic arrangements of spins, respectively. These two states have a long range order. The spin arrangement of *Figure 4.9c* is an example with no long-range order. Within the one-electron band picture, the ferromagnetic state *Figure 4.9a* is represented by the electronic structure that results when all the band levels are singly occupied with an identical spin, as depicted in *Figure 4.10a*, which is a solid state analog of the dimer high-spin state *Figure 4.8c*. If one neglects electron-electron repulsion terms except for the on-site and the nearest-neighbor intersite Coulomb repulsions, the electronic energies of the three states *Figures 4.9a-4.9c* are identical. Consequently, the high-spin band filling scheme *Figure 4.10a* represents any localized electronic state arising from a half-filled band.

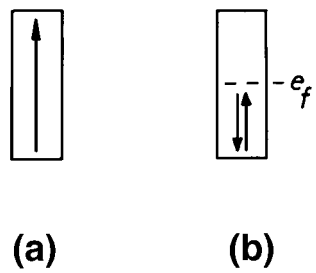

Figure 4.10. Band orbital pictures of the (a) magnetic insulating state and (b) normal metallic state of a system with half filled band.

It is difficult to describe the energies for the low-lying excited states of a Mott-Hubbard localized state (e.g., the energy differences between the states, *Figures 4.9a-4.9c*) within a band electronic structure theory, because this theory is based upon the assumption that electrons are delocalized throughout the lattice. Localized electronic systems are typically examined in terms of model Hamiltonians (e.g., spin and Hubbard Hamiltonians) designed to study their low-lying excited states.

For a half-filled metallic system, the low-spin band filling in *Figure 4.10b* is appropriate when U << W. This is a solid state analog of the dimer low-spin state in *Figure 4.8b*. The energies for the low-lying excited states of the metallic state *Figure 4.10b* are well described by the band orbital energy differences in the vicinity of the Fermi level.

For a solid in which U ≈ W, it is difficult to predict whether a metallic or a magnetic insulating state is more stable. In certain cases the total energy is lowered by introducing spin polarization on each lattice site (i.e., $n\uparrow > n\downarrow$ or $n\uparrow < n\emptyset$), because it reduces the contribution of on-site repulsion to the total energy. This leads to a magnetic metallic state, which has weakly localized electrons. It is important to consider how spin polarization can be introduced in a band picture. Since each band level can have up-spin and down-spin electrons, one can consider that each band is made up of two subbands, i.e., one band for up-spin electrons, and the other band for down-spin electrons. For example, *Figure 4.11a* depicts a normal metallic state in this picture, where e_{f0} refers to the Fermi

level of the normal metallic state. Spin polarization can be introduced into a normal metallic state by shifting the up-spin band with respect to the down-spin band.[13] For simplicity, it may be assumed that the spatial orbital character of these subbands is essentially unaffected by the spin polarization. With respect to the normal metallic state (*Figure 4.11a*), one can obtain more up-spin electrons by raising the Fermi level to $e_{f0} + \Delta\uparrow$, and less down-spin electrons by lowering the Fermi level to $e_{f0} - \Delta\downarrow$ (*Figure 4.11b*). When the up-spin and down-spin bands are shifted so that the $e_{f0} + \Delta\uparrow$ and $e_{f0} - \Delta\downarrow$ levels become identical (i.e., adjusted to the new Fermi level e_f), a spin-polarized state results (*Figure 4.11c*). The electronic state of *Figure 4.11c* represents a magnetic metallic state.[13] In this picture, the case for U >> W is represented by the state in which the up-spin and down-spin bands are completely separated (*Figure 4.11d*). Thus the up-spin is completely filled while the down-spin band is completely empty thereby representing a magnetic insulating state. The states represented by *Figures 4.10a* and *4.11d* are equivalent.

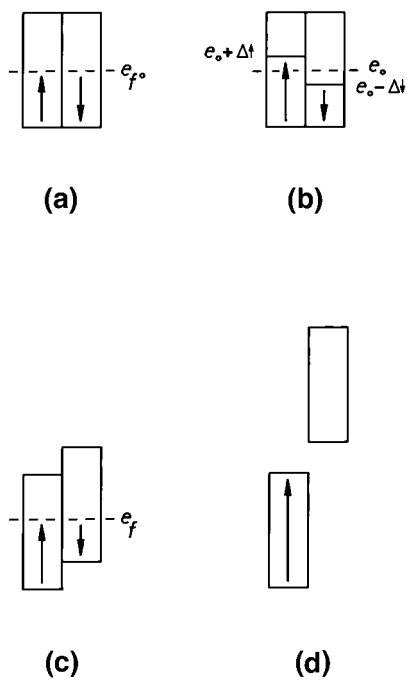

Figure 4.11. Up-spin and down-spin subband representations of the various states of a system with a half-filled band. (a) Normal metallic state. (b) Electron redistribution in the up-spin and down-spin subbands. (c) Spin polarized state. (d) Magnetic insulating state.

4.6.2 Normal metallic states and Fermi surfaces

For the metallic state of a partially filled band, wave vectors in a certain region of the FPZ lead to occupied band levels (i.e., levels below the Fermi level), and wave vectors in the remaining region of the FPZ lead to unoccupied band levels (i.e., levels above the Fermi level). For simplicity, wave vectors leading to occupied and unoccupied levels of a partially filled band are referred to as occupied and unoccupied wave vectors, respectively. All wave vectors of the FPZ are equally probable, so that the occupancy of a partially filled band is equal to the ratio of the area of the occupied wave vectors to that of the FPZ. The Fermi surface of a partially filled band is the boundary surface separating the occupied wave vectors from the unoccupied wave vectors, i.e., the surface made up of the Fermi wave vectors $\mathbf{k}_f$.

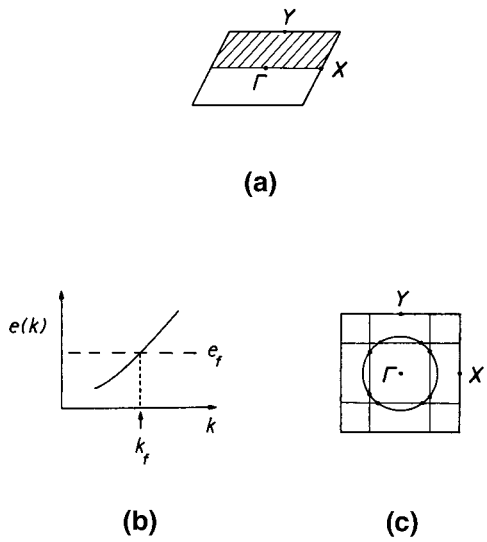

Figure 4.12. (a) FPZ of a non-orthorhombic 2D lattice. (b) Dispersion relation of a band across the Fermi level. (c) Schematic illustration of how to determine a Fermi surface.

We examine how to calculate a Fermi surface first by considering the normal metallic state of a 2D system as an example. To make our discussion general, this 2D system will be assumed to be non-orthorhombic, so that the FPZ are given by a parallelogram (*Figure 4.12a*). Suppose the n-th band is partially filled. With a set of k-points $\{k_1, k_2, \cdots, k_L\}$ covering one half the FPZ (indicated by shading in *Figure 4.12a*), the Fermi level e_f can be determined. Given the n-th band energies $e_n(\mathbf{k}_i)$ calculated for this set of k-points, one can generate an analytical expression of $e_n(\mathbf{k})$ as a function of $\mathbf{k}$ by a 2D cubic spline fitting procedure.[14] For this fitting purpose the FPZ is more useful than the FBZ because the former provides a much simpler set of evenly distributed k-points. Once an analytical expression of $e_n(\mathbf{k})$ and the Fermi level e_f are obtained, it is easy to find the Fermi vector $\mathbf{k}_f$, for which $e_n(\mathbf{k}_f) = e_f$, along any wave vector direction desired (see *Figure 4.12b*). To present a Fermi surface as a contour in the FPZ, one needs to find a large number of $\mathbf{k}_f$ values. This is achieved by examining the dispersion relations of the band $e_n(\mathbf{k})$ along several sets of parallel wave vector lines dividing the FPZ. This is illustrated with two sets of parallel wave vector lines in *Figure 4.12c*, where the $\mathbf{k}_f$ points found are represented by heavy dots. If one applies a finer mesh of parallel wave vector lines, more $\mathbf{k}_f$ points are found. Then, the Fermi surface is given by the contour line connecting those $\mathbf{k}_f$ points as shown by the solid line in *Figure 4.12c*.

The above discussion can be easily extended for a 3D system. The 3D FPZ of a 3D crystal can be sliced by a set of cross sections parallel to the a*b*-, b*c*- or a*c*-plane. For each cross-section plane, 2D Fermi surface contours can be calculated as described above. When these contours on all cross-section planes are collected, one obtains the Fermi surfaces of the 3D system.

A Fermi surface is made up of the Fermi wave vectors $\mathbf{k}_f$, and the crystal momentum $\hbar\mathbf{k}_f$ shows the direction of electron movement on the Fermi surface. In other words, there exists a nonzero carrier density for electrical conduction along the direction perpendicular to the Fermi surface. Therefore, in a representation of a Fermi surface using wave vectors in all three directions, a 1D metal has two Fermi surface sheets perpendicular to the direction of its electrical conduction, a 2D metal has a cylinder-like Fermi surface running along the direction of the least electrical conductivity, and a 3D metal has a completely closed Fermi surface.

4.6.3 Effective mass

The energy of a free electron $\varepsilon(\mathbf{k})$ is given by

$$\varepsilon(\mathbf{k}) = \frac{(\hbar\mathbf{k})^2}{2m_e} \tag{4.72}$$

where m_e is the mass of an electron. Given the energy of a partially band as $e_i(\mathbf{k})$, it is convenient to describe its behavior around the Fermi level in terms of a parabolic relationship

$$e_i(\mathbf{k}) = \frac{(\hbar\mathbf{k})^2}{2m^*} \tag{4.73}$$

Here the effective mass m^* is used to describe any deviation of the band $e_i(\mathbf{k})$ from the free electron behavior $\varepsilon(\mathbf{k})$. In general, dispersion relations of a band depend on the directions of wave vectors, and so do the effective mass. For a Fermi surface in a 2D FPZ or for a Fermi surface on a cross-section plane of a 3D FPZ, it is convenient to consider the average effective mass defined by [15]

$$m^* = \frac{\hbar^2}{2\pi}\frac{dA}{de} \tag{4.74}$$

where A refers to the area of either the occupied or the unoccupied wave vector region of the 2D FPZ or the cross-section plane of the 3D FPZ.

4.7 States derived from a metallic state [5,16]

4.7.1 Fermi surface nesting

Fermi surfaces are important in explaining the electronic instabilities of partially filled band systems. When a piece of a Fermi surface can be translated by a vector **q** and superimposed on another piece of the Fermi surface, the Fermi surface is said to be nested by the vector **q**. Since the Fermi surface of *Figure 4.13a* consists of two parallel lines, it is nested by an infinite number of wave vectors, two examples of which are shown in *Figure 4.13a*. For the discussion of Fermi surface nesting, it is important to consider Fermi surfaces in the entire reciprocal space, which is achieved by repeating the Fermi surface pattern of the FPZ in reciprocal space.

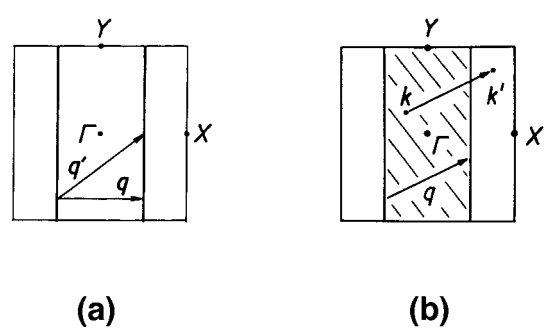

Figure 4.13. (a) Nesting vectors of a 1D Fermi surface. (b) Filled and empty wave vectors of the FPZ given by a 1D Fermi surface, where the filled region is indicated by shading.

4.7.2 Orbital mixing and new states

In discussing metal-insulator and metal-superconductor transitions, it is convenient to describe the insulating and the superconducting states as a consequence of perturbation on the metallic state. A metallic state predicted by one-electron band theory (i.e., a normal metallic state) is not stable when its Fermi surface is nested, and becomes susceptible to a metal-insulator transition under a suitable perturbation. We now examine the nature of the nonmetallic states that are derived from a normal metallic state upon mixing its occupied and unoccupied band levels. In *Figure 4.13b*, the occupied wave vector region is indicated by shading, and the vector **q** is one of many possible nesting vectors. To simplify our notations, the occupied and unoccupied wave vectors are denoted by **k** and **k'**, respectively. Each unit cell will be assumed to contain one atomic orbital χ, so the Bloch orbitals ϕ defined in Eq. 4.50 are the crystal orbitals as well. Suppose we choose the **k** and **k'** values to satisfy the relationship

$$\mathbf{q} = \mathbf{k} - \mathbf{k'} \tag{4.75}$$

The orbitals $\phi(\mathbf{k})$ and $\phi(\mathbf{k'})$ are eigenfunctions of the unperturbed Hamiltonian H^o. If a certain perturbation H' is introduced, these orbitals may not be eigenfunctions of H^o + H' anymore, so that they interact to give modified orbitals $\psi(\mathbf{k})$ and $\psi(\mathbf{k'})$

$$\begin{aligned} \psi(\mathbf{k}) &\propto \phi(\mathbf{k}) + \gamma\,\phi(\mathbf{k'}) \\ \psi(\mathbf{k'}) &\propto -\gamma\ \phi(\mathbf{k}) + \phi(\mathbf{k'}) \end{aligned} \tag{4.76}$$

where γ is a mixing coefficient. These orbital mixings are possible when the interaction matrix elements $\langle\phi(\mathbf{k})|H'|\phi(\mathbf{k'})\rangle$ are nonzero. If the **k** and **k'** values are chosen from the Fermi surface, then $\phi(\mathbf{k})$ and $\phi(\mathbf{k'})$ are degenerate. In other cases, $\phi(\mathbf{k})$ and $\phi(\mathbf{k'})$ are nondegenerate, but the energy difference between $\phi(\mathbf{k})$ and $\phi(\mathbf{k'})$ becomes smaller as **k** approaches the Fermi surface.

The electron density distributions associated with $\psi(\mathbf{k})$ and $\psi(\mathbf{k'})$ are given by

$$\begin{aligned} \psi(\mathbf{k})\psi^*(\mathbf{k}) &\propto \phi(\mathbf{k})\phi^*(\mathbf{k}) + \gamma^2\,\phi(\mathbf{k'})\phi^*(\mathbf{k'}) + \Delta\rho \\ \psi(\mathbf{k'})\psi^*(\mathbf{k'}) &\propto \gamma^2\,\phi(\mathbf{k})\phi^*(\mathbf{k}) + \phi(\mathbf{k'})\phi^*(\mathbf{k'}) - \Delta\rho \end{aligned} \tag{4.77}$$

where

$$\Delta\rho = \gamma\,[\phi^*(\mathbf{k})\phi(\mathbf{k'}) + \phi(\mathbf{k})\phi^*(\mathbf{k'})] \tag{4.78}$$

If we expand $\phi^*(\mathbf{k})\phi(\mathbf{k'})$ and $\phi(\mathbf{k})\phi^*(\mathbf{k'})$ using Eq. 4.50 and keep only the diagonal terms $\chi(\mathbf{r}-\mathbf{R})\chi^*(\mathbf{r}-\mathbf{R})$, it can be shown that

$$\Delta\rho \propto \sum_{\mathbf{R}} \cos(\mathbf{q}\cdot\mathbf{R})\chi(\mathbf{r}-\mathbf{R})\chi^*(\mathbf{r}-\mathbf{R}) \tag{4.79}$$

Therefore, with respect to $\phi(\mathbf{k})$ or $\phi(\mathbf{k'})$, $\psi(\mathbf{k})$ and $\psi(\mathbf{k'})$ each have density wave character whose periodicity in real space is governed by the term $\cos(\mathbf{q}\cdot\mathbf{R})$. According to Eqs. 4.77 and 4.79, $\psi(\mathbf{k})$ leads to density accumulation where $\psi(\mathbf{k'})$ has density depletion, and vice versa. If the density distribution arising from $\phi(\mathbf{k})$ or $\phi(\mathbf{k'})$ is represented by a straight line, then the density accumulation and depletion associated with $\phi(\mathbf{k})$ and $\phi(\mathbf{k'})$ occur as a wave form as shown in *Figure 4.14*, where shaded and unshaded half waves represent density accumulation and depletion, respectively.

Suppose that the orbital mixings defined in Eq. 4.79 are carried out for all occupied **k** of the FPZ under the condition **q** = **k** - **k'** to obtain sets of modified orbitals $\{\psi(\mathbf{k})\}$ and $\{\psi(\mathbf{k'})\}$ from sets of unmodified orbitals $\{\phi(\mathbf{k})\}$ and $\{\phi(\mathbf{k'})\}$. The normal metallic state is one in which all the $\phi(\mathbf{k})$ orbitals are doubly occupied. Then as illustrated in *Figure 4.15a* for a 1D chain, each site has no magnetic

moment and has an identical amount of charge. A charge density wave (CDW) state occurs when the $\psi(\mathbf{k})$ orbitals are doubly occupied. As illustrated in *Figure 4.15b* for a 1D chain, a CDW state has no local magnetic moment but charge densities on atomic sites vary in a wave manner. When $\psi(\mathbf{k})$ and $\psi(\mathbf{k'})$ are each singly occupied by up-spin and down-spin electrons, respectively, a spin density wave (SDW) state results. As shown in *Figure 4.15c* for 1D chain, the SDW state has a local magnetic moment at atomic sites but the total charge density on each atomic site is identical.

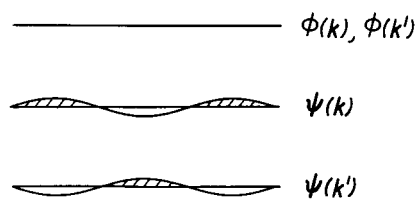

Figure 4.14. Density wave formation that results when a filled orbital $\phi(k)$ interacts with the empty orbital $\phi(k')$s related by the nesting vector $q = k' - k$.

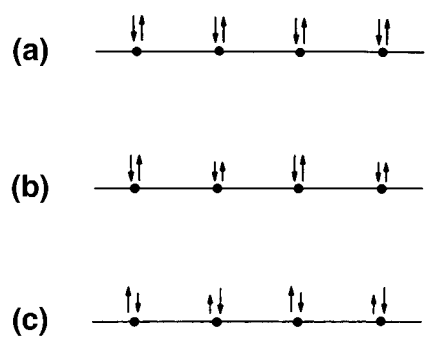

Figure 4.15. Electron distributions at the lattice sites of a 1D chain with one electron per site in various electronic states. (a) Metallic state, (b) CDW state, (c) SDW state.

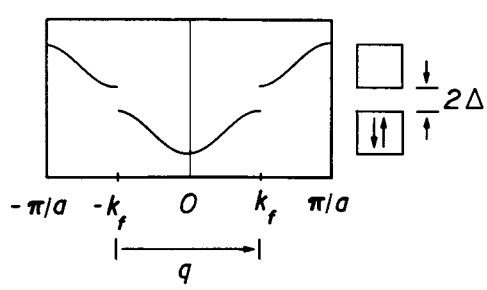

Figure 4.16. Effect of a CDW formation on the dispersion relation and the energy band of a 1D system with a half filled.

Unless $\phi(\mathbf{k})$ and $\phi(\mathbf{k'})$ are degenerate, which occurs when **k** is on the Fermi surface, the mixing of the unoccupied orbital $\phi(\mathbf{k'})$ into the occupied level $\phi(\mathbf{k})$ has an energy-raising effect, although it

can be more than compensated by the energy lowering associated with the interaction energy $<\phi(\mathbf{k})|H'|\phi(\mathbf{k'})>$. Thus the orbital mixing between $\phi(\mathbf{k})$ and $\phi(\mathbf{k'})$ becomes more favorable as the energy difference between them decreases, i.e., when the **k** value approaches the Fermi surface. As illustrated in *Figure 4.16* for a partially filled 1D band system, the orbital mixing between $\phi(\mathbf{k})$ and $\phi(\mathbf{k'})$ changes their energies in the vicinity of the Fermi level most significantly and opens a band gap at the Fermi level. In *Figure 4.16* the band gap is given by 2Δ, where $\Delta = <\phi(\mathbf{k})|H'|\phi(\mathbf{k'})>$ evaluated for $\mathbf{k} = \mathbf{k}_f$. When there exists a Fermi surface nesting, the favorable orbital mixing can be achieved for a large region of **k**-values in the vicinity of the Fermi surface. This explains why a metal with nested Fermi surface is susceptible toward a phase transition that leads to orbital mixing between the levels around the Fermi level thereby creating a band gap.

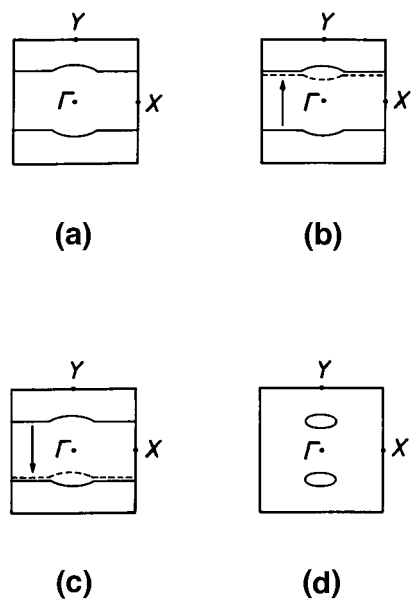

Figure 4.17. Schematic diagrams illustrating the effect of a CDW formation on the Fermi surface in case of an incomplete Fermi surface nesting.

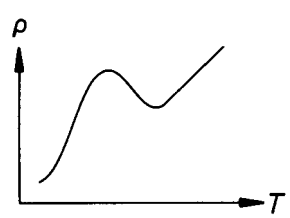

Figure 4.18. Resistivity-versus-temperature plot showing a metal-to-semiconductor-to-metal phase transition.

By definition, Fermi surfaces disappear when a band gap opens at the Fermi level. So far in our discussion, a complete Fermi surface nesting (e.g., *Figure 4.13a*) has been assumed. In such a case, all the Fermi surface is removed by an appropriate orbital mixing. In certain cases, a Fermi surface nesting may be incomplete, as illustrated in *Figure 4.17a*, if some parts of the Fermi surface have different curvatures. In this case, only the nested portion of the surface is removed by orbital mixing as

illustrated in *Figures 4.17b* and *4.17c*, so that the unnested portion is left as small Fermi surface pockets as shown in *Figure 4.17d*, which represents a metallic state. Compared with *Figure 4.17a*, *Figure 4.17d* has a smaller Fermi surface area and hence a smaller number of carriers (i.e., those electrons at the Fermi level). Suppose that a phase transition induced by temperature lowering gives rise to the Fermi surface change from *Figure 4.17a* to *Figure 4.17d*. Such a phase transition is likely to exhibit a resistivity-versus-temperature plot as shown in *Figure 4.18*. However, if a Fermi surface nesting is complete, *Figure 4.1c* will be observed.

4.7.3 CDW instability

So far we have implicitly assumed that a band level below e_f is completely filled (i.e., occupancy of 1), and that above e_f is completely empty (i.e., occupancy of 0). This picture is valid for all levels when T = 0, but only for the levels lying outside the vicinity of the Fermi level (e.g., $e < e_f - 4k_BT$ and $e > e_f + 4k_BT$, where k_B is the Boltzmann constant) when T > 0. For the levels lying close to the Fermi level (e.g., $e_f - 4k_BT < e < e_f + 4k_BT$), whose orbital mixing plays a crucial role in lowering the energy of a metal with nested Fermi surface, thereby leading to a metal-insulator transition, their orbital occupancy f(e) at nonzero temperature is given by the Fermi-Dirac distribution function

$$f(e) = \frac{1}{1 + \exp\left(\frac{e - e_f}{k_B T}\right)} \tag{4.80}$$

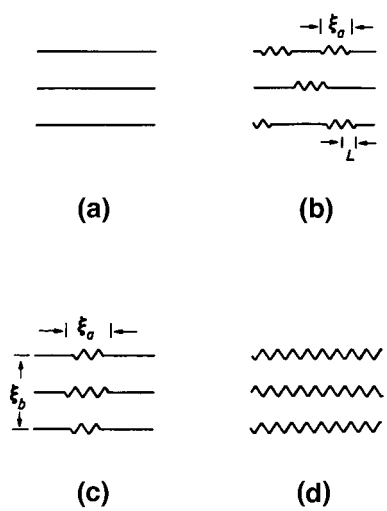

Figure 4.19. Schematic diagrams illustrating the effect of temperature on the CDW formation in individual chains of a 1D metallic system. (a) $T > T_{1D}$, (b) $T_{1D} > T > T_X$, (c) $T_C < T < T_X$, and (d) $T < T_C$.

Thus, f(e) < 1 for $e < e_f$, and f(e) > 0 for $e > e_f$. For example, in the vicinity of the Fermi level of *Figure 4.13b*, the occupancy of $\phi(\mathbf{k})$ is less than 1, and that of $\phi(\mathbf{k'})$ is larger than 0 (at T > 0). Consequently, the energy gain resulting from the orbital mixing between $\phi(\mathbf{k})$ and $\phi(\mathbf{k'})$ is maximum at T = 0 and decreases as T is raised. Thus, only when T is lowered below a certain temperature does the energy gain associated with the orbital mixing become substantial enough to cause a metal-insulator transition.

Metal-insulator transition arising from a CDW instability is not abrupt, but typically undergoes a series of steps.[17] This process can be illustrated by considering a 1D metal as composed of weakly interacting chains. At a high temperature, each chain has no tendency for CDW formation, so all chains have uniform density distributions, as illustrated by straight lines in *Figure 4.19a*. Below a certain temperature T_{1D}, each chain has a tendency for CDW formation. As depicted in *Figure 4.19b*, a CDW is formed and destroyed dynamically at many parts of each chain, and CDW formation in one chain is independent of those in other chains. The average length of a CDW segment (i.e., coherence length) is ξ_a. At a certain temperature T_x below T_{1D}, CDW segments among different chains begin to order along the interchain direction as shown in *Figure 4.19c*, where ξ_b is the coherence length along the interchain direction. Finally, at a certain temperature T_c below T_x, CDW formation in each chain is complete and CDW's among different chains are ordered, as shown in *Figure 4.19d*. Therefore, a long range order sets in. The coherence lengths ξ_a and ξ_b increase gradually upon lowering the temperature as the extents of long-range order along the intra- and interchain directions increase. These coherence lengths become infinite when a long-range order is complete in both directions.

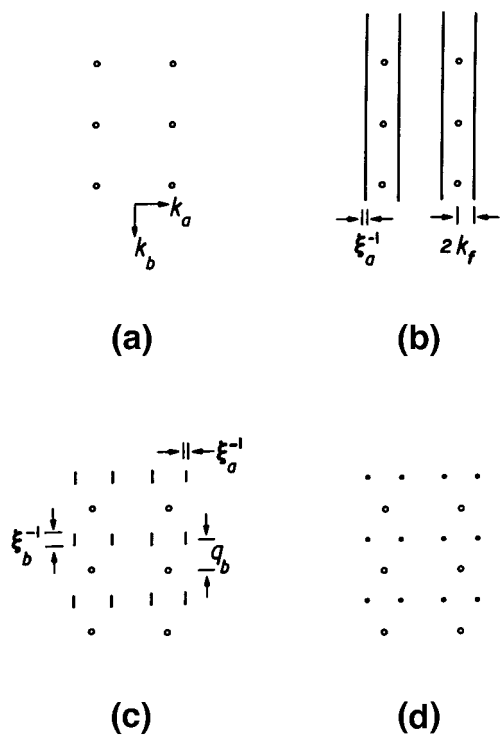

Figure 4.20. Schematic diagrams illustrating the diffraction patterns that correspond to the various temperature regimes of Figures 3.19a-d: (a) $T > T_{1D}$, (b) $T_{1D} > T > T_x$, (c) $T_c < T < T_x$, and (d) $T < T_c$.

The temperature dependence of CDW formation in real space, discussed above, is deduced typically from single-crystal X-ray diffraction measurements.[17] At $T > T_{1D}$, the diffraction pattern of a 1D metal shows only Bragg peaks, as shown in *Figure 4.20a*. At $T_x < T < T_{1D}$, the diffraction pattern shows diffuse lines (or sheets in 3D representation) perpendicular to the k_a-direction, which are located at $\pm q_a$ (i.e., $\pm 2k_f$) from the rows of the Bragg peaks, as shown in *Figure 4.20b*. The thickness of the diffuse line is given by ξ_a^{-1}. At $T_c < T < T_x$, the diffuse lines are transformed into diffuse spots

(or rods in 3D representation) centered at ($2k_f$, q_b) and its equivalent positions, as shown in *Figure 4.20c*. The thicknesses of a diffuse spot along the k_a- and k_b-directions are given by ξ_a^{-1} and ξ_b^{-1}, respectively. Below $T < T_c$, a long-range order sets in so that the diffuse spots are converted into superlattice spots, as shown in *Figure 4.20d*. The diffuse spot thicknesses along the intra- and interchain directions are inversely proportional to the coherence lengths x_a and ξ_b, respectively. Thus the diffuse spots become smaller as the extent of long-range order along the two directions increases, and eventually become superlattice spots after a long-range order sets in along both directions.

The perturbation causing the CDW state associated with a nesting vector **q** is a lattice vibration with the wave vector **q**. When the CDW state is formed, the lattice distorts so that the lattice vibration of wave vector **q** is softened. Consequently, the vibrational energy band shows a frequency lowering in the vicinity of the nesting value **q** as shown in *Figure 4.21*, which is known as the Kohn anomaly.[18] For a Fermi surface consisting of parallel lines (in 2D representation) as in *Figure 4.13b*, an infinite number of nesting vectors **q** are present. However, only one specific **q** value is likely to be adopted by the partially-filled band system because distortion induces lattice strain. Thus the chosen **q** value is the one that leads to an optimum energy lowering for the system by balancing the electronic energy gain and the lattice strain. When CDW vectors **q** are integer fractions (i.e., 1/2, 1/3, 1/4, etc.) of reciprocal lattice vectors, the CDW's are said to be commensurate. Otherwise, they are called incommensurate.

The perturbation causing the CDW state associated with a nesting vector **q** is a lattice vibration with the wave vector **q**. When the CDW state is formed, the lattice distorts so that the lattice vibration of wave vector **q** is softened. Consequently, the vibrational energy band shows a frequency lowering in the vicinity of the nesting value **q** as shown in *Figure 4.21*, which is known as the Kohn anomaly.[18] For a Fermi surface consisting of parallel lines (in 2D representation) as in *Figure 4.13b*, an infinite number of nesting vectors **q** are present. However, only one specific **q** value is likely to be adopted by the partially-filled band system because distortion induces lattice strain. Thus the chosen **q** value is the one that leads to an optimum energy lowering for the system by balancing the electronic energy gain and the lattice strain. When CDW vectors **q** are integer fractions (i.e., 1/2, 1/3, 1/4, etc.) of reciprocal lattice vectors, the CDW's are said to be commensurate. Otherwise, they are called incommensurate.

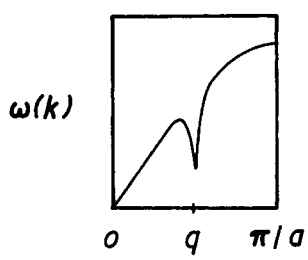

Figure 4.21. Kohn anomaly associated the CDW formation associated with the nesting vector q.

4.7.4 Superconducting state [19]

When the temperature is lowered, a metal may become susceptible to another type of electronic instability, i.e., formation of a superconducting state. For a metal to become superconducting, it should avoid the electronic instability toward a metal-insulator transition leading to a CDW or an SDW state. In general, the Fermi surface of a 1D metal is well-nested, so a 1D metal rarely undergoes a metal-superconductor transition. From the viewpoint of one-electron band theory, a superconducting state also involves orbital mixing among band levels above and below the Fermi level. However, the way this orbital mixing comes about is quite different from that discussed for CDW and SDW states.[16c,19c]

Charge carriers of a superconducting state are not individual electrons as in a normal metallic state, but pairs of electrons (called Cooper pairs) having opposite momenta (i.e., opposite wave vectors). Thus, Cooper pairs are described by product functions $\phi(\mathbf{k})\phi(-\mathbf{k})$ and $\phi(\mathbf{k'})\phi(-\mathbf{k'})$, where **k** and **k'** refer to occupied and unoccupied wave vectors of a normal metallic state, respectively.[16c,19c] The energy lowering that brings about superconductivity is induced by the interaction of an occupied pair function $\phi(\mathbf{k})\phi(-\mathbf{k})$ with an unoccupied pair function $\phi(\mathbf{k'})\phi(-\mathbf{k'})$, i.e., $\langle\phi(\mathbf{k})\phi(-\mathbf{k})|H'|\phi(\mathbf{k'})\phi(-\mathbf{k'})\rangle$, where the perturbation H' causing this mixing is electron-phonon interaction in traditional superconductors described by the BCS theory.[19] As a consequence of the interaction between the pair functions, the character of the unoccupied pair function is mixed into that of the occupied pair function. In this indirect way, a superconducting state incorporates unoccupied orbital character into the occupied orbital character. Interactions between the pair functions $\phi(\mathbf{k})\phi(-\mathbf{k})$ and $\phi(\mathbf{k'})\phi(-\mathbf{k'})$ introduce an energy gap at the Fermi level, as do the interactions between $\phi(\mathbf{k})$ and $\phi(\mathbf{k'})$ in forming CDW and SDW states. It should be recalled that charge carriers of a superconducting state are Cooper pairs. A superconducting energy gap prevents Cooper pairs from breaking up when there is no excitation energy greater than the gap. The latter is a few multiples of k_BT_C at absolute zero temperature, where T_C is the superconducting transition temperature, and gradually decreases to zero at T_C.

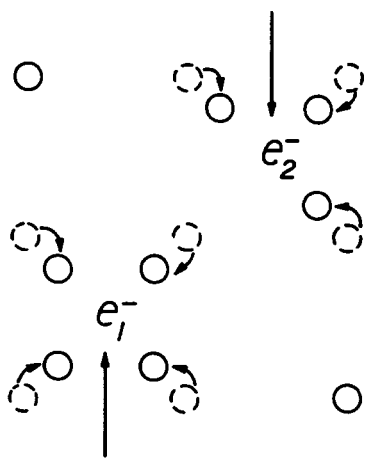

Figure 4.22. Schematic diagram showing the formation of a Cooper pair (i.e., the charge carrier of a superconducting state) as a result of electron-phonon coupling.

For traditional superconductors, Cooper pair formation is induced by electron-phonon interaction:[19] As depicted in *Figure 4.22*, a moving electron causes a slight, momentary lattice deformation around itself. The deformation affects the motion of a second electron (moving in the opposite direction) in the wake of the first in such a way that, effectively, the two electrons move as an entity as if bound together by an attractive force. The extent of electron-phonon coupling is measured by the electron-phonon coupling constant λ. The superconducting transition temperature T_C and the coupling constant λ are governed by the expression [19b]

$$T_C \approx \frac{\Theta}{1.45} \exp\left[-\frac{1.04(1+\lambda)}{\lambda + \mu^*(1+0.5\lambda)}\right] \quad (4.81)$$

where Θ is the Debye temperature and μ^* is the effective Coulomb pseudopotential, which is of the order of 0.1. Among the factors affecting the magnitude of T_C in Eq. 4.81, the most important one is

the electron-phonon coupling constant λ. In general, T_c increases with increasing λ. For a lattice with atoms of mass M and with a vibrational band conducive for electron-phonon coupling, the constant λ is given by [19b]

$$\lambda = \frac{n(e_f)\langle I^2 \rangle}{M\langle \omega^2 \rangle} \tag{4.82}$$

where $\langle I^2 \rangle$ is the square of the electron-phonon interaction element averaged over the Fermi surface, and $\langle \omega^2 \rangle$ is the square of the phonon frequency averaged over the vibrational band. The $M\langle \omega^2 \rangle$ term has the dimension of a force constant, so a large λ results when the lattice has a low-frequency phonon spectrum (i.e., soft phonons arising from vibrations with shallow potential wells). Therefore, when the lattice is soft toward the low-frequency phonons crucial for superconductivity, the electron-phonon coupling constant λ is large, thereby raising the T_c.[20]

Certainly, for a superconducting state to occur, the energy increase associated with the introduction of unoccupied orbital character should be smaller than the energy gain resulting from interaction among Cooper pair functions. Depending upon the nature and strength of the perturbations causing orbital mixing, a normal metallic state with nested Fermi surface may lead to a superconducting state when the temperature is lowered if CDW or SDW formation associated with the nesting can be prevented. Such a case occurs when the interaction matrix elements $\langle \phi(\mathbf{k})|H'|\phi(\mathbf{k'})\rangle$ responsible for CDW or SDW formation are small compared with the interaction matrix elements $\langle \phi(\mathbf{k})\phi(-\mathbf{k})|H'|\phi(\mathbf{k'})\phi(-\mathbf{k'})\rangle$ that cause a superconducting state. When the relative stabilities of CDW, SDW, and superconducting states are similar, preference of one state over the other is delicately balanced by a change in temperature and pressure.[21]

References

1. Mott, N. F., *Conduction in Non-Crystalline Materials, Oxford University Press*, New York, 1987.
2. (a) Whangbo, M.-H., *J. Chem. Phys*. **1979**, *70*, 4963.
   (b) Whangbo, M.-H., *Inorg. Chem*. **1980**, *19*, 1728.
   (c) Whangbo, M.-H., in *Extended Linear Chain Compounds, Vol. 2*; Miller, J. S., ed.: Plenum, New York, 1982, p. 127.
3. (a) Whangbo, M.-H.; Schlegel, H. B.; Wolfe, S. *J. Am. Chem. Soc*. **1977**, *99*, 1296.
   (b) Whangbo, M.-H. in *Computational Theoretical Organic Chemistry*; Daudel, R.; Csizmadia, I. G., eds.: Reidel, Boston, 1981, p. 233.
   (c) Albright, T. A.; Burdett, J. K.; Whangbo, M.-H., *Orbital Interactions in Chemistry*; Wiley, New York, 1985.
4. Hughbanks, T.; Hoffmann, R. *J. Am. Chem. Soc*. **1983**, *105*, 3528.
5. Canadell, E.; Whangbo, M.-H., *Chem. Rev*., **1991**, *91*, 965.
6. Hoffmann, R. *J. Chem. Phys*. **1963**, *39*, 1397.
7. (a) Clementi, E.; Roetti, C. *Atomic Data Nuclear Data Tables*, **1974**, *14*, 177.
   (b) McLean, A. D.; McLean, R. S. *Atomic Data Nuclear Data Tables*, **1981**, *26*, 197.
   (c) Richardson, J. W.; Blackman, M. J.; Ranochak, J. E. *J. Chem. Phys*. **1973**, *58*, 3010.
8. Wolfsberg, M.; Helmholz, L. *J. Chem. Phys*. **1952**, *20*, 837.
9. (a) Ballhausen, C. J.; Gray, H. B. Molecular Orbital Theory; Benjamin: New York, 1965.
   (b) Basch, H.; Viste, A.; Gray, H. *Theoret. Chim. Acta* **1965**, *3*, 458.
   (c) Basch, H.; Viste, A.; Gray, H. *J. Chem. Phys*. **1966**, *44*, 10.
   (d) Baranovskii, V.; Nikolskii, A. *Theor. Eksp. Khim*. **1967**, *3*, 527.
10. (a) Ammeter, J. H.; Bürgi, H. -B.; Thibeault, J.; Hoffmann, R. *J. Am. Chem. Soc*. **1978**, *100*, 3686.
    (b) Whangbo, M.-H.; Hoffmann, R. *J. Chem. Phys*. **1978**, *68*, 5498.
11. (a) Whangbo, M.-H.; Hoffmann, R., *J. Am. Chem. Soc*. **1978**, *100*, 6093.

(b) Whangbo, M.-H.; Hoffmann, R.; Woodward, R. B., *Proc. Roy. Soc., London, Ser. A*, **1979**, *366*, 23.

12. (a) Mott, N. F. *Metal-Insulator Transitions*; Barnes and Noble: New York, 1977.
(b) Brandow, B. H. *Adv. Phys*. **1977**, *26*, 651.
13. Seo, D.-K.; Whangbo, M.-H. *J. Am. Chem. Soc*. **1996**, *118*, 3951.
14. Press, W. H.; Flannery, B. P.; Teukolsky, S. A.; Vetterling, W. T. *Numerical Recipes*; Cambridge University Press: New York, 1987.
15. D. Shoenberg, *Magnetic Oscillations in Metals*, Cambridge University Press, Cambridge, 1984.
16. (a) Whangbo, M. -H. *J. Chem. Phys*. **1980**, *73*, 3854.
(b) Whangbo, M. -H. *Acc. Chem. Res*. **1983**, *16*, 95.
(c) Whangbo, M.-H., *Adv. Chem. Ser*. **1989**, *226*, 269.
17. Pouget, J. P., *Low-Dimensional Electronic Properties of Molybdenum Bronzes and Oxides;* Schlenker, C., Ed.; Kluwer: Dordrecht, The Netherlands, 1989; p. 87.
18. (a) Kohn, W. *Phys. Rev. Lett*. **1959**, *2*, 393.
(b) Kagoshima, S. *Extended Linear Chain Compounds*; Miller, J. S., ed.; Plenum: New York, 1982; Vol. 2, Ch. 7.
19. (a) Bardeen, J.; Cooper, L. N.; Schrieffer, J. R. *Phys. Rev*. **1957**, 108, 1175.
(b) McMillan, W. L. *Phys. Rev*. **1968**, *167*, 331.
(c) Solymar, L.; Walsh, D., Lectures on the Electrical Properties of Materials, 5th Edition; Oxford University Press, Oxford, 1993; Ch. 14.
20. (a) Whangbo, M. -H.; Williams, J. M.; Schultz, A. J.; Emge, T. J.; Beno, M. A. *J. Am. Chem. Soc*. **1987**, *109*, 90.
(b) Williams, J. M.; Ferraro, J. R.; Thorn, R. J.; Carlson, K. D.; Geiser, U.; Wang, H. H.; Kini, A. M.; Whangbo, M. -H. *Organic Superconductors*; Prentice Hall, New York, 1992.
21. Nasu, K. *J. Phys. Soc. Jpn*. **1985**, *54*, 1933.